

# Electron viscosity, current vortices and negative nonlocal resistance in graphene

Leonid Levitov<sup>1</sup> and Gregory Falkovich<sup>2</sup>

<sup>1</sup> Department of Physics, Massachusetts Institute of Technology, Cambridge, Massachusetts 02139, USA and

<sup>2</sup> Weizmann Institute of Science, Rehovot 76100 Israel

Quantum-critical states of diverse strongly correlated systems are predicted to feature universal collision-dominated transport resembling that of viscous fluids. However, investigation of these phenomena has been hampered by the lack of known macroscopic signatures of the hydrodynamic regime at criticality. Here we identify vorticity as such a signature and link it with an easily verifiable striking macroscopic transport behavior. Produced by the viscous flow, vorticity can drive electric current against an applied field, resulting in a negative nonlocal voltage. We argue that the latter plays the same role for the viscous regime as zero electrical resistance does for superconductivity. Besides offering a diagnostic of viscous transport which distinguishes it from ohmic currents, the sign-changing electrical response affords a robust tool for directly measuring the viscosity-to-resistivity ratio. The strongly interacting electron-hole plasma in high-mobility graphene provides a bridge between quantum-criticality and the cornucopia of fluid mechanics phenomena.

Symmetries play central role in developing our understanding of strongly interacting states of matter[1]. Symmetry approach proved particularly fruitful for many systems of current interest, ranging from quantum-critical states in solids and ultracold atomic gases to quark-gluon plasmas.[2–5] These systems share common long-wavelength behavior originating from the fundamental symmetries of space-time and respective conservation laws of energy and momentum. Hydrodynamics, which has taken a central stage in these developments, serves as a framework helping to reveal the universal collective behavior. Powerful approaches based on conformal field theory and AdS/CFT duality grant the well-established notions of fluid mechanics, such as viscosity and vorticity, an entirely new dimension.[6, 7]

However, despite their prominence and new paradigmatic role, viscous flows in strongly correlated systems have so far lacked directly verifiable macroscopic transport signatures. Surprisingly, this has been the case even for condensed matter systems where a large variety of experimental techniques is available to probe collective behaviors.[8–10] Identifying a signature that would do to viscous flows what zero electrical resistance did to superconductivity has remained an outstanding problem. The goal of this article is to point out that vorticity generated in viscous flows leads to a unique macroscopic transport behavior that can serve as an unambiguous diagnostic of the viscous regime. Namely, we predict that vorticity of the shear flows generated by viscosity can result in a backflow of electrical current that can *run against the applied field*, see Fig.1. The resulting negative nonlocal voltage can serve as a clear signature of the collective viscous behavior. Associated with it are characteristic sign-changing spatial patterns of electric potential (see Fig.1 and Fig.2) which can be used to directly image vorticity and shear flows in electron systems with modern capacitance scanning microscopy techniques.[11, 12]

The negative electrical response, which is illustrated in Fig.1, originates from basic properties of shear flows.

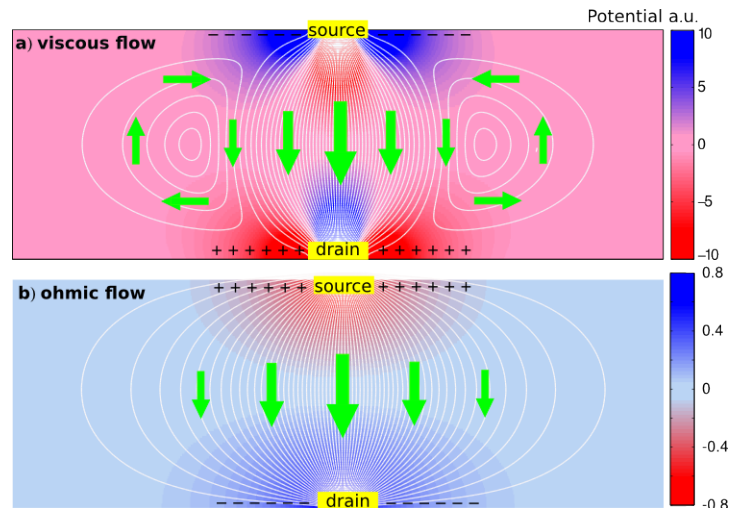


FIG. 1: Current streamlines and potential map for viscous and ohmic flows. White lines show current streamlines, colors show electrical potential, arrows show the direction of current. Panel a) presents the mechanism of a negative electrical response: Viscous shear flow generates vorticity and a back flow on the side of the main current path, which leads to charge buildup of the sign opposing the flow and results in a negative nonlocal voltage. Streamlines and electrical potential are obtained from Eq.(5) and Eq.(6). The resulting potential profile exhibits multiple sign changes and  $\pm 45^\circ$  nodal lines, see Eq.(7). This provides directly measurable signatures of shear flows and vorticity. Panel b) shows that, in contrast, ohmic currents flow down the potential gradient, producing a nonlocal voltage in the flow direction.

We recall that the collective behavior of viscous systems results from particles rapidly exchanging momenta in two-body collisions while maintaining the net momentum conserved. Since momentum remains a conserved quantity collectively, it gives rise to a hydrodynamic momentum transport mode. This mode describes momentum flow in space, diffusing transversely to the source-drain current flow and away from the nominal current path. A

shear flow established as a result of this process generates vorticity and (for an incompressible fluid) a back flow in a direction reverse to the applied field. Such a complex and manifestly non-potential flow pattern has a direct impact on the electrical response. In particular, a finite momentum density in field-free space regions will drive charge flow which is unaccompanied by electric field. The latter will produce charge buildup, generating electric fields tending to stop the current and thus acting opposite to the field driving the source drain-current. Interestingly, as discussed in detail below, only a shear flow but not the backflow is required for a negative electric field to build up in the system. This assures the pervasive nature of the negative electrical response which persists even in the presence of a fairly significant ohmic currents (see Fig.2).

Attempts to connect electron theory with fluid mechanics have a long and interesting history. Early work on viscosity of Fermi liquids made connection with ultrasound damping.[13] Subsequently, Gurzhi introduced an electronic analog of Poiseuille flow.[14] Related temperature dependent phenomena in nonlinear transport were observed by deJong and Molenkamp.[15] Theory of a hydrodynamic, collision-dominated regime was further developed by Damle and Sachdev in the context of quantum-critical states of strongly-interacting systems.[2] An important step was made by Andreev, Kivelson, and Spivak[10] who argued that hydrodynamic contributions can dominate resistivity in systems with a large disorder correlation length. In a recent work Davison, Schalm, and Zaanen argued that electron viscosity is key for understanding the famous linear resistivity of the normal state of the copper oxides.[16] These ideas were followed up in an angle resolved photoemission study of cuprate superconductors.[17] Recently, a ‘viscometer’ comprised of an AC-driven Corbino disc was proposed.[9] In each of these cases, however, a model-dependent analysis was required to delineate the effects of viscosity from ‘extraneous’ contributions. In contrast, the nonlocal response considered here is directly sensitive to the collective momentum transport mode which underpins viscous flow, therefore providing an unambiguous diagnostic of the viscous regime.

To clarify this point we note that, since momentum density is independent of electrical charge, viscous electronic flow is described by an inherently charge-neutral mode. Therefore, momentum transport cannot, in itself, result in charge and electric field buildup. The latter occurs only when streamlines run into system boundary, contacts, or some other inhomogeneity, as in Fig.1. Recently, nonlocal electrical response mediated by chargeless modes was shown to be uniquely sensitive to the quantities which are not directly accessible in electrical transport measurements, in particular spin currents and valley currents.[18–20] In a similar manner, the nonlocal response discussed here gives a diagnostic of viscous transport which is more direct and powerful than any

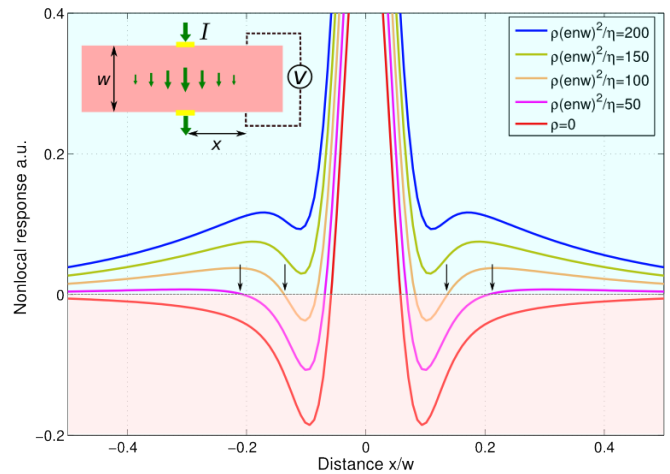


FIG. 2: Nonlocal response for different resistivity-to-viscosity ratios  $\rho/\eta$ . Plotted is voltage  $V(x)$  at a distance  $x$  from current leads obtained from Eq.(12) for the setup shown in the inset. The voltage is positive in the ohmic-dominated region at large  $|x|$  and negative in the viscosity-dominated region closer to the leads (positive values at even smaller  $|x|$  reflect the finite contact size  $a \approx 0.05w$  used in simulation). Viscous flow dominates up to fairly large resistivity values, resulting in negative response persisting up to values as large as  $\rho(ew)^2/\eta \approx 120$ . Nodal points, marked by arrows, are sensitive to the  $\rho/\eta$  value, which provides a way to directly measure viscosity (see text).

approaches based on local transport.

The quantum-critical behavior is predicted to be particularly prominent in graphene.[21–23] Electron interactions in graphene are strengthened near charge neutrality (CN) due to the lack of screening at low carrier densities.[23, 24] As a result, carrier collisions are expected to dominate transport in pristine graphene in a wide range of temperatures and dopings.[25] Furthermore, estimates of electronic viscosity near CN yield one of the highest known viscosity-to-entropy ratios which approaches the universal bound for strongly interacting systems inferred from the AdS/CFT correspondence.[8] These developments fueled further interest in electronic viscosity in graphene.[9, 26, 27]

To show that the timescales are favorable, we will use parameter values estimated for pristine graphene samples which are almost defect free, such as free-standing graphene.[28] Kinematic viscosity can be estimated as momentum diffusion coefficient  $\nu \approx \frac{1}{2}v_F^2\gamma_{ee}^{-1}$  where  $\gamma_{ee}$  is the carrier-carrier scattering rate, and  $v_F = 10^6$  m/s for graphene. Refs.[23, 24] estimate this rate as  $\gamma_{ee} \approx A\alpha^2k_B T/\hbar$ , where  $\alpha$  is the interaction strength. For  $T = 100$  K, approximating the prefactor as  $A \approx 1$ [23, 24], we obtain characteristic times,  $\gamma_{ee}^{-1} \approx 70$  fs. Disorder scattering can be estimated from the measured mean free path values which reach a few microns at large doping [29]. Using the momentum relaxation rate square-root dependence on doping,  $\gamma_p \propto n^{-1/2}$ , and extrapo-

lating to charge neutrality,  $n \sim 10^{10} \text{ cm}^{-2}$ , gives times  $\gamma_p^{-1} \sim 0.5 \text{ ps}$ , which are much longer than the values  $\gamma_{ee}^{-1}$  estimated above. The inequality  $\gamma_p \ll \gamma_{ee}$  justifies our hydrodynamical description of transport.

Momentum transport in the hydrodynamic regime is described by continuity equation for momentum density,

$$\partial_t p_i + \partial_j T_{ij} = -\gamma_p p_i, \quad T_{ij} = P\delta_{ij} + \mu v_i v_j + T_{ij}^{(v)}, \quad (1)$$

where  $T_{ij}$  is the so-called stress tensor describing momentum flow,  $P$  and  $\mu$  are pressure and mass density, and  $\mathbf{v}$  is the carrier drift velocity. The quantity  $\gamma_p$  describes electron-lattice momentum relaxation due to disorder or phonons, which we will assume to be small compared to the electron-electron collision rate. For systems at degeneracy, we can relate pressure to the electrochemical potential via  $P = en\Phi$  with  $n$  the particle number density. Viscosity contributes to the stress tensor via

$$T_{ij}^{(v)} = \eta(\partial_i v_j + \partial_j v_i) + (\zeta - \eta)\partial_k v_k \delta_{ij} \quad (2)$$

where  $\eta$  and  $\zeta$  are the first and second viscosity coefficients. For incompressible flows, which describe transport in charged systems at drift velocities smaller than plasmonic velocities, the velocity field is divergenceless,  $\partial_i v_i = 0$ . This, at linear order in  $\mathbf{v}$ , leads to an electronic Navier-Stokes (NS) equation

$$\partial_t p_i - \eta \nabla^2 v_i + \gamma_p p_i = -\partial_i P. \quad (3)$$

This equation describes momentum transport: imparted by the external field  $\mathbf{f} = -\nabla P$ , momentum flows to system boundary where dissipation takes place. It is therefore important to endow Eq.(3) with suitable boundary conditions. In fluid mechanics this is described by the no-slip boundary condition  $\mathbf{v} = 0$ . It is instructive to generalize this condition to account for partial slippage:

$$v_{\perp} = 0, \quad v_{\parallel} = -\alpha \partial_{\parallel} P \quad (4)$$

where the subscripts  $\perp$  and  $\parallel$  indicate the velocity and derivative components normal and tangential to the boundary. The width of the boundary layer is on the order of the carrier mean free path  $l = v/\gamma_{ee}$ .

As a quick illustration, consider current flowing down a long strip of a finite width. A steady viscous flow features a nonuniform profile in the strip cross-section governed by momentum flow to the system boundary. Eq.(3), applied to a strip  $0 < y < w$ , yields  $(-\eta \partial_y^2 + \gamma_p mn)v(y) = enE$ , where  $v(y)$  and  $E$  are the drift velocity and electric field directed along the strip (and  $m$  is an effective mass defined through the relation  $\mathbf{p} = mn\mathbf{v}$ ). Setting  $\alpha$  and  $\gamma_p$  to zero for simplicity, we find a parabolic profile  $v(y) = Ay(w - y)$ , where  $A = neE/2\eta$  and  $\eta = mn\nu$ . The nonzero shear  $\partial_y v = A(w - 2y)$  describes momentum flow to the boundary. The net current  $I = \int_0^w nev(y')dy' = (n^2 e^2/12\eta)w^3 E$  scaling as a cube of the strip width is the electronic analog of the Poiseuille

law. Being distinct from the linear scaling  $I \propto wE$  in the ohmic regime, the cubic scaling can in principle be used to identify the viscous regime. It is interesting to put the current-field relation in a ‘‘Drude’’ form using kinematic viscosity:  $I = \frac{ne^2 \tau_w}{m} wE$  with  $\tau_w = w^2/12\nu$  an effective scattering time. Evaluating the latter as  $\tau_w \approx \frac{1}{6}(w/v_F)^2 \gamma_{ee}$  we find values that, for realistic system parameters, can greatly exceed  $\gamma_p^{-1}$ . This remarkable observation was first made in Ref. [14].

Next, we proceed to analyze nonlocal response in a strip with transverse current injected through a pair of point-like current leads as pictured in Fig.1. Unlike the above case of longitudinal current, here the potential profile is not set externally but must be obtained from (3). We begin with introducing a stream function via  $\mathbf{v} = \mathbf{z} \times \nabla \psi$ , which solves the flow incompressibility condition. At first we will completely ignore the ohmic effects, setting  $\alpha$  and  $\gamma_p$  to zero as above, which leads to a biharmonic equation  $(\partial_x^2 + \partial_y^2)^2 \psi = 0$  with the boundary conditions  $v_x = 0$ ,  $nev_y = I\delta(x)$  for  $y = 0, w$ . Using Fourier transform in  $x$ , we write  $\psi(x, y) = (2\pi)^{-1} \int dk e^{ikx} \psi_k(y)$  and then determine  $\psi_k(y)$  separately for each  $k$  as in the above warm-up problem. Inverting Fourier transform gives stream function

$$\psi(x, y) = \frac{I}{ne} \int \frac{dk e^{ikx}}{2\pi ik} [(y \sinh k\tilde{y} + \tilde{y} \sinh ky) a_k + b_k(y)] \quad (5)$$

where we defined  $\tilde{y} = w - y$ ,  $a_k = k \tanh(kw/2)/(kw + \sinh kw)$ ,  $b_k(y) = (e^{ky} + e^{k(w-y)})/(e^{kw} + 1)$ . Contours (isolines) of  $\psi$  give the streamlines for the flow shown in Fig.1. While most of them are open lines connecting source and drain, some streamlines form loops. The latter define vortices occurring on both sides of the current path. Numerically we find that vortex centers are positioned very close to  $x = \pm w$ , see Appendix.

We can now explore electrical potential of viscous flow. The latter can be found directly from  $\psi(x, y)$  giving

$$\phi(x, y) = \frac{\beta I}{2} \int dk e^{ikx} a_k [\sinh k(y - w) + \sinh ky], \quad (6)$$

where we defined  $\beta = 2\eta/(\pi n^2 e^2)$  (see Appendix). As illustrated in Fig.1, Eq.(6) predicts a peculiar sign-changing spatial dependence, with two pairs of nodal lines crossing at contacts. To understand this behavior, we evaluate  $\phi(x, y)$  explicitly in the regions near contacts  $(x, y) = (0, 0), (0, w)$ . Near the first contact, approximating  $\tanh(kw/2) \approx \text{sgn } k$ ,  $\sinh ky \approx \frac{1}{2} e^{|k|y} \text{sgn } k$ , etc, we find

$$\phi(x, y) \approx \frac{\beta I}{2} \int dk e^{ikx} |k| e^{-|k|y} = \frac{\beta I (y^2 - x^2)}{(y^2 + x^2)^2} \quad (7)$$

( $|x|, |y| \ll w$ ). Eq.(7) predicts an inverse-square dependence vs. distance from contacts and also a presence of two nodal lines running at  $\pm 45^\circ$  angles relative to the

nominal current path. Similar behavior is found near the other contact,  $\phi(x, y) \approx -\frac{\beta((w-y)^2-x^2)}{((w-y)^2+x^2)^2}I$ . We note that the  $r^{-2}$  power law dependence is much stronger than the  $\ln r$  dependence expected in the ohmic regime. This, as well as multiple sign changes, provides clear signatures of a viscous flow.

The nonlocal voltage measured at a finite distance from the current leads (see schematic in Fig.2 inset) can be evaluated as  $V(x) = \phi(x, w) - \phi(x, 0)$ . From Eq.(7) we predict voltage that is falling off as  $x^{-2}$  and is of a *negative sign*:

$$V(x) \approx -\frac{2\beta}{x^2}I \quad (8)$$

( $|x| \lesssim w$ ). Microscopically, negative voltage originates from a viscous shear flow which creates vorticity and backflow on both sides of the current path, see Fig.1.

Numerically we see that the negative response persists to arbitrarily large distances, see  $\rho = 0$  curve in Fig.2. The sign change at very short  $x$ , evident in Fig.2, arises due to a finite contact size. We model it by replacing the delta function in the boundary condition for current source by a Lorentzian,  $nev_y = Ia/\pi(x^2 + a^2)$  at  $y = 0, w$ . After making appropriate changes in the above derivation (namely, plugging  $e^{-a|k|}$  under the integral) we find

$$V(x) \approx -\frac{\beta I}{(x-ia)^2} + \text{c.c.} = -\frac{2\beta I(x^2 - a^2)}{(x^2 + a^2)^2} \quad (9)$$

This expression exhibits a sign change at  $x = a$  and is negative for all  $|x| > a$ .

It is interesting to clarify to what extent the negative response is sensitive to boundary conditions, in particular to the no-slip assumption. Extending the above analysis to the partial-slip boundary conditions in Eq.(4) we find the nonlocal response of the form

$$V(x) = \beta I \int dk e^{ikx} \frac{k \tanh(kw/2) \sinh kw}{kw + (1 + \tilde{\alpha}k^2) \sinh kw}, \quad (10)$$

where  $\tilde{\alpha} = 2\eta\alpha/ne$ . The expression under the integral represents an even function of  $k$  with a zero at  $k = 0$  and a symmetric double-peak structure. The peaks roll off at  $|k| \sim \tilde{\alpha}^{-1/2}$ , producing a UV cutoff of the integral similar to that for the above model of a finite-size contact. Our numerical analysis shows that this is indeed the case, with a finite  $\alpha$  translating into an effective contact size  $a \approx \tilde{\alpha}^{1/2}$ . In other words, the partial-slip boundary conditions can alter the response only very close to the contact while rendering it unaffected at larger distances.

So far we ignored the bulk momentum relaxation, setting  $\gamma_p = 0$  in Eq.(3). We now proceed to show that the signatures of viscous flow identified above are robust in the presence of a background ohmic resistivity  $\rho = m\gamma_p/ne^2$  so long as it is not too strong. The dimensionless parameter which governs the respective roles of

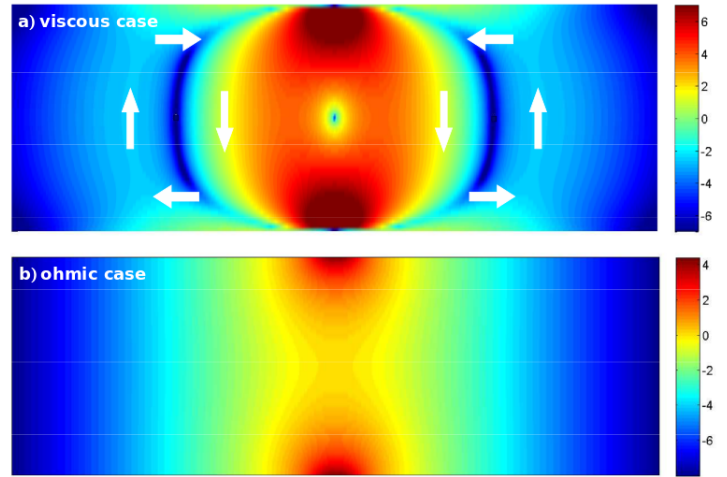


FIG. 3: Dissipated heat for viscous and ohmic flows. Viscous flow (panel a) results in a highly complex heating pattern with intense hot spots near contacts and cold arc-shaped patches at vortices surrounded by warmer regions. (Also note a cold spot at the center where the flow is locally uniform and thus  $W = 0$ , see Eq.(13)). White arrows show current direction. Ohmic flow (panel b) shows an essentially featureless heat production rate  $W \sim |(\partial_x + i\partial_y)\psi|^2$  decaying monotonously away from contacts.

resistivity vs. viscosity is

$$\epsilon = \rho(new)^2/\eta \approx 2\gamma_{ee}\gamma_p(w/v_F)^2. \quad (11)$$

For the values  $\gamma_{ee}$  and  $\gamma_p$  quoted above, and taking  $w = 1 \mu\text{m}$ , one obtains  $\epsilon \sim 10$ . Incorporating finite resistivity in the calculation is uneventful (see Appendix), yielding a response

$$V(x) = I \int \frac{dk}{\pi k} \frac{\rho e^{ikx} (e^{qw} - 1)(e^{kw} - 1)q}{q_+ (e^{qw} - e^{kw}) + q_- (e^{qw} e^{kw} - 1)}, \quad (12)$$

where  $q^2 = k^2 + \epsilon w^{-2}$ ,  $q_{\pm} = q \pm k$ . For  $\epsilon = 0$  we recover the above viscous result, which is negative, whereas for  $\epsilon \rightarrow \infty$  Eq.(12) gives the well-known ohmic result  $V(x) = \frac{\rho}{\pi} \ln [\coth(\pi x/2w)]$ , which is positive. With both  $\eta$  and  $\rho$  nonzero, the resistance given by Eq.(12) is positive at large  $x$  but remains negative close to the contact even at fairly high resistivity values corresponding to  $\epsilon \lesssim 100$ , see Fig.2. The positions of the nodes, marked by arrows in Fig.2, have strong dependence on the ratio  $\rho/\eta$ , which provides a convenient way to directly measure the electronic viscosity.

The pervasive character of negative nonlocal response can be understood by noting that viscosity, being a coefficient of the highest derivative term in Eq.(3), dominates at short distances  $x \lesssim x_* = \sqrt{\eta/\rho(en)^2}$ . Such robustness, manifest in Fig.2, will facilitate experimental detection of viscous transport.

Vorticity of a viscous flow also manifests itself in heat production

$$W = \eta (\partial_i v_j + \partial_j v_i)^2 = 2\eta |(\partial_x + i\partial_y)^2 \psi(x, y)|^2 \quad (13)$$

The heating pattern shown in Fig.3 features hot spots near contacts and cold arc-shaped elongated patches in vorticity regions. In contrast, for an ohmic flow the pattern is essentially featureless. This makes viscous flows an interesting system to explore with the nanoscale temperature scanning techniques.[30]

We finally note that there are tantalizing parallels—both conceptual and quantitative—between electronic viscous flows and current microfluidics systems. E.g. Eq.(3) describes the low-Reynolds (microfluidic) flow between two plates separated by a distance  $h$ , provided  $\gamma_p = 12\nu/h^2$ . A new research area at the frontier of nanoscience and fluid mechanics, microfluidics aims to manipulate and control fluids at a nanoscale with the ultimate goal of developing new lab-on-a-chip microtechnologies. Graphene, which can be easily patterned into any shapes without compromising its excellent qualities, can become a basis of electronic microfluidics, with multiple applications in information processing and nanoscale charge and energy transport that remain to be explored.

- 
- [1] S. Sachdev, *Quantum Phase Transitions* (Cambridge University Press, Cambridge, UK, 2001).
- [2] K. Damle, S. Sachdev, Nonzero-temperature transport near quantum critical points *Phys. Rev. B* **56**, 8714 (1997).
- [3] P. K. Kovtun, D. T. Son, A. O. Starinets, Viscosity in Strongly Interacting Quantum Field Theories from Black Hole Physics *Phys. Rev. Lett.* **94**, 111601(2005)
- [4] D. T. Son, Vanishing Bulk Viscosities and Conformal Invariance of the Unitary Fermi Gas *Phys. Rev. Lett.* **98**, 020604 (2007)
- [5] K. Karsch, D. Kharzeev, K. Tuchin, Universal properties of bulk viscosity near the QCD phase transition *Physics Letters B* **663**, 217-221 (2008)
- [6] D. T. Son, A. O. Starinets, Viscosity, black holes, and quantum field theory, *Annual Review of Nuclear and Particle Science*, **57**, 95118 (2007).
- [7] S. Sachdev, M. Muller, Quantum criticality and black holes, *J. Phys. Condensed Matter*, **21**, Article ID 164216, 2009.
- [8] M. Müller, J. Schmalian, L. Fritz, Graphene: A Nearly Perfect Fluid *Phys. Rev. Lett.* **103** 025301 (2009)
- [9] A. Tomadin, G. Vignale, M. Polini, Corbino Disk Viscometer for 2D Quantum Electron Liquids *Phys. Rev. Lett.* **113**, 235901 (2014)
- [10] A. V. Andreev, S. A. Kivelson, B. Spivak Hydrodynamic Description of Transport in Strongly Correlated Electron Systems *Phys. Rev. Lett.* **106**, 256804 (2011)
- [11] M. J. Yoo, T. A. Fulton, H. F. Hess, R. L. Willett, L. N. Dunkleberger, R. J. Chichester, L. N. Pfeiffer, K. W. West, Scanning Single-Electron Transistor Microscopy: Imaging Individual Charges *Science* **276**, 579-582 (1997)
- [12] A. Yacoby, H.F. Hess, T.A. Fulton, L.N. Pfeiffer, K.W. West, Electrical imaging of the quantum Hall state *Solid State Communications* **111** 1-13 (1999)
- [13] E.M. Lifshitz & L.P. Pitaevskii, *Physical Kinetics* (Pergamon Press 1981)
- [14] R. N. Gurzhi, Hydrodynamic Effects in Solids at Low Temperature *Usp. Fiz. Nauk* **94**, 689 [*Sov. Phys. Usp.* **11**, 255 (1968)].
- [15] M. J. M. de Jong, L. W. Molenkamp, Hydrodynamic electron flow in high-mobility wires *Phys. Rev. B* **51**, 13389-13402 (1985)
- [16] R. A. Davison, K. Schalm, J. Zaanen, Holographic duality and the resistivity of strange metals *Phys. Rev. B* **89**, 245116 (2014).
- [17] J. D. Rameau, T. J. Reber, H.-B. Yang, S. Akhanjee, G. D. Gu, P. D. Johnson, S. Campbell, Nearly perfect fluidity in a high-temperature superconductor *Phys. Rev. B* **90**, 134509 (2014)
- [18] D. A. Abanin, R. V. Gorbachev, K. S. Novoselov, A. K. Geim, L. S. Levitov, Giant Spin-Hall Effect Induced by the Zeeman Interaction in Graphene *Phys. Rev. Lett.* **107**, 096601 (2011)
- [19] D. A. Abanin, S. V. Morozov, L. A. Ponomarenko, R. V. Gorbachev, A. S. Mayorov, M. I. Katsnelson, K. Watanabe, T. Taniguchi, K. S. Novoselov, L. S. Levitov, A. K. Geim, Giant nonlocality near the Dirac point in graphene *Science* **332**, 328330 (2011).
- [20] R. V. Gorbachev, J. C. W. Song, G. L. Yu, A. V. Kretinin, F. Withers, Y. Cao, A. Mishchenko, I. V. Grigorieva, K. S. Novoselov, L. S. Levitov, A. K. Geim, Detecting topological currents in graphene superlattices *Science* **346**, 448-451 (2014)
- [21] J. González, F. Guinea, M.A.H. Vozmediano, Non-Fermi liquid behavior of electrons in the half-filled honeycomb lattice (A renormalization group approach) *Nucl. Phys. B* **424**, 595 (1994).
- [22] D.E. Sheehy, J. Schmalian, Quantum Critical Scaling in Graphene *Phys. Rev. Lett.* **99**, 226803 (2007)
- [23] L. Fritz, J. Schmalian, M. Müller, S. Sachdev Quantum critical transport in clean graphene *Phys. Rev. B*, **78** 085416 (2008).
- [24] A.B. Kashuba, Conductivity of Defectless Graphene *Phys. Rev. B*, **78** 085415 (2008).
- [25] B. N. Narozhny, I. V. Gornyi, M. Titov, M. Schütt, A. D. Mirlin, Hydrodynamics in graphene: Linear-response transport *Phys. Rev. B* **91**, 035414 (2015)
- [26] A. Principi, G. Vignale, M. Carrega, M. Polini, Bulk and shear viscosities of the 2D electron liquid in a doped graphene sheet arXiv:1506.06030
- [27] A. Cortijo, Y. Ferreirós, K. Landsteiner, M. A. H. Vozmediano, Hall viscosity from elastic gauge fields in Dirac crystals arXiv:1506.05136
- [28] K.I. Bolotin, K. J. Sikes, Z. Jiang, M. Klima, G. Fudenberg, J. Hone, P. Kim, H. L. Stormer, Ultrahigh electron mobility in suspended graphene *Solid State Comm.* **146**, 351-355 (2008).
- [29] T. Taychatanapat, K. Watanabe, T. Taniguchi, P. Jarillo-Herrero (2013) Electrically tunable transverse magnetic focusing in graphene *Nature Physics*, **9** 225.
- [30] G. Kucsko, P. C. Maurer, N. Y. Yao, M. Kubo, H. J. Noh, P. K. Lo, H. Park & M. D. Lukin Nanometre-scale thermometry in a living cell *Nature* **500**, 54-58 (2013)

## SUPPLEMENTARY MATERIAL

We start by reminding the reader that for ohmic transport the current-field relation is local and, as a result,

current is a potential vector field which has zero vorticity. Indeed  $\mathbf{j} = \sigma \mathbf{E}$  with  $\mathbf{E} = -\nabla\phi$ , where  $\phi$  is electrostatic potential, yields  $\nabla \times \mathbf{j} = 0$ . Expressing current density through particle number density and flow velocity,  $\mathbf{j} = nev$ , and assuming constant carrier concentration  $n$ , we see that the velocity field itself is potential. Combining this with the continuity equation gives  $\nabla_i v_i = \Delta\phi = 0$ . Incompressibility allows one to introduce the stream function via  $(v_x, v_y) = (-\partial_y\psi, \partial_x\psi)$ . The quantity  $\psi$  in the ohmic case also satisfies the Laplace equation  $\Delta\psi = 0$ .

In contrast, the flow of a viscous fluid is described by the Navier-Stokes and continuity equations

$$\eta\Delta v_i = ne\nabla_i\phi, \quad \nabla_i v_i = 0, \quad (14)$$

where  $\eta$  is the dynamic viscosity. The velocity field of a viscous flow is generally not potential as the vorticity  $\omega = \Delta\psi$  is non-zero, since the stream function is not harmonic (as in the Ohmic case) but rather bi-harmonic function inside the domain:

$$\Delta^2\psi = 0. \quad (15)$$

This equation is of fourth-order so it needs extra boundary conditions apart from those imposed on the normal velocity (i.e. entering and exiting current). For a viscous fluid, as long as one accounts for the momentum exchange among carriers, one needs to account for an exchange with the solid boundary as well. We start from the simplest case of the no-slip condition,  $\nabla_n\psi = 0$ , and show straightforward modification for partial slippage at the end. Imposing also  $\nabla_l\psi = 0$  everywhere on the boundary except current-carrying electrodes, we need to find  $\psi, v, \phi$ , then relate the current  $I$  to the voltage  $U = \phi_3 - \phi_4$  and find the resistance  $R_{12,34}$ .

Using the complex variable  $z = x + iy$ , a general solution of the bi-harmonic equation (15) can be written in a compact form:  $\psi(x, y) = \bar{z}f(z) + g(z)$ . In particular, for a strip of width  $w$  in  $y$  and infinite in  $x$ , we get

$$\psi(x, y) = \frac{1}{2\pi} \int dk e^{ikx} \psi_k(y), \quad (16)$$

We consider here the case of the current driven across the strip, entering and exiting at the center,  $v_y(x, 0) = v_y(x, w) = \partial_x\psi = I\delta(x)/en$ , so that  $\psi_k(0) = \psi_k(w) = -I/enk$ . No-slip condition  $v_x(x, 0) = v_x(x, w) = 0$  gives  $\partial_y\psi_k(0) = \partial_y\psi_k(w) = 0$ . We then obtain:

$$\psi(x, y) = \frac{I}{ne} \int \frac{dk}{2\pi} \frac{e^{ikx}}{ik} \left\{ \frac{\cosh k(y - w/2)}{\cosh kw/2} + \frac{k \tanh kw/2}{kw + \sinh kw} [y \sinh k(w - y) + (w - y) \sinh ky] \right\}. \quad (17)$$

That formula describes the current, which flows along the lines  $\psi(x, y) = \text{const}$ , shown by white lines in the upper panel of Figure 1 (see main text). Note that (17)

is singular at the current-carrying electrodes, i.e. at  $(x \rightarrow 0, y \rightarrow 0, w)$ , that singularity comes from the integrand tending to a constant at  $k \rightarrow \infty$ . Ultraviolet regularization of this expression can be done either by introducing a small finite electrode size or a small slip, as discussed at the end, the salient features of Figure 1 (see main text) are independent of regularization. The most remarkable feature of (17) is that it describes two extremum points  $(\pm x_0, w/2)$  determined by the condition  $\partial_x\psi(x, w/2) = 0$ , which gives (denoting  $kw = 2t$ )

$$\int dt \cos(2tx_0/w) [1 + 2t \tanh t \sinh t / (2t + \sinh 2t)] = 0. \quad (18)$$

Apparently,  $x_0 \simeq w$ . Those two points are the centers of the vortices seen in Figure 1 (see main text).

The terms in  $\psi$ , which are purely exponential in  $y$ , are harmonic and turn  $\Delta\psi$  into zero. Those terms do not contribute to the potential  $\phi$ :

$$\phi(x, y) = \frac{I\eta}{\pi(ne)^2} \int dk e^{ikx} a_k [\sinh k(y - w) + \sinh ky] \quad (19)$$

where  $a_k = k \tanh(kw/2)/(kw + \sinh kw)$ . The spatial profile of the potential for the viscous case has a remarkable behavior which is illustrated in the upper panel of Figure 1 (see main text). The potential is zero on the line  $y = w/2$  by symmetry. Yet only for sufficiently small  $x$ , i.e. close to the center, the potential goes from negative to positive as one increases  $y$ . Away from the center, the potential difference is actually reversed. In particular, the potential along the edges has the sign opposite to the potential of the respective electrode. Indeed, let us determine the voltage  $V(x) = \phi(w, x) - \phi(0, x)$  at the pair of points, which are distance  $x$  away from the current-bearing electrodes:

$$V(x) = \frac{2I\eta}{\pi(ne)^2} \int dk e^{ikx} \frac{k \tanh(kw/2) \sinh kw}{kw + \sinh kw}. \quad (20)$$

The voltage is a Fourier transform of a positive function, which is symmetric with respect to  $k \rightarrow -k$ , has a zero at  $k = 0$  and grows as  $|k|$  as  $k \rightarrow \infty$ . We infer that the voltage and the resulting resistance  $R(x) = U(x)/I$  are negative for any  $x$ . Indeed, at  $x \ll w$ , the integral (20) is determined by  $k > 1/w$ :  $R \approx -4\eta/\pi(nex)^2$ . As  $x$  increases,  $|V(x)|$  monotonically decreases to zero. The reason for the negative nonlocal voltage is a viscous vortex backflow seen in the upper panel of Figure 1 (see main text).

An expression for the heat production rate due to viscous friction is given by

$$W = \eta \sum_{ik} (\partial_i v_k + \partial_k v_i)^2 = 2\eta [4\psi_{xy}^2 + (\psi_{xx} - \psi_{yy})^2] = 2\eta |(\partial_x + i\partial_y)^2 \psi|^2. \quad (22)$$

For (17) we have

$$(\partial_x + i\partial_y)^2 \psi(x, y) = \frac{I\nu}{n\epsilon\pi} \int k dk e^{ikx} \left\{ \frac{e^{k(y-w/2)}}{\cosh kw/2} + \frac{\tanh kw/2}{kw + \sinh kw} \left[ [1 + k(y-w)]e^{ky} + (1 + ky)e^{k(y-w)} \right] \right\} \quad (23)$$

The map of heat production described by (22,23) is shown in the upper panel of the Figure 3 of the main text, where the lower panel shows the heat production due to Ohmic resistance,  $\rho(n\epsilon\nu)^2$ . The radical difference between the two maps can serve as yet another signatory, allowing one to distinguish the viscous regime with three minima (one between the electrodes and two inside vortices) from the Ohmic regime with a single maximum (between the electrodes) and a monotonic decay with  $|x|$ . Note also the much wider hot regions around the electrodes, again manifesting nonlocality of the viscous case.

Let us now account for both Ohm resistance and viscosity acting together:

$$[\eta\Delta^2 - \rho(en)^2\Delta]\psi = 0. \quad (24)$$

The same equation describes the low-Reynolds (microfluidic) flow between two plates separated by the distance  $h$ , where  $\rho(en)^2 = 12\eta/h^2$ . For a strip, one looks for the solution of (24) in the form (16), so that (24) takes the form

$$(\partial_y^2 - k^2)(\partial_y^2 - q^2)\psi_k = 0 \quad q^2 = k^2 + \rho(en)^2/\eta. \quad (25)$$

Apparently, nonzero  $\rho$  lifts the degeneracy of the eigenvalues so the solution is a sum of the four exponents:

$$\psi_k = -\frac{I}{en\epsilon k} [a_{\pm} \exp(\pm ky) + b_{\pm} \exp(\pm qy)]. \quad (26)$$

Boundary conditions

$$\begin{aligned} a_+ e^{kw} + a_- e^{-kw} + b_+ e^{qw} + b_- e^{-qw} &= 1, \\ a_+ + a_- + b_+ + b_- &= 1, \quad k(a_+ - a_-) + q(b_+ - b_-) = 0, \\ ka_+ e^{kw} - ka_- e^{-kw} + qb_+ e^{qw} - qb_- e^{-qw} &= 0. \end{aligned}$$

fix the factors:

$$\begin{aligned} a_+ &= \frac{(e^{qw} - 1)q}{(k - q)(1 - e^{(k+q)w}) + (k + q)(e^{qw} - e^{kw})}, \\ a_- &= \frac{e^{kw}(e^{qw} - 1)q}{(k - q)(1 - e^{(k+q)w}) + (k + q)(e^{qw} - e^{kw})}, \\ b_+ &= \frac{(e^{kw} - 1)k}{(q - k)(1 - e^{(k+q)w}) + (k + q)(e^{kw} - e^{qw})}, \\ b_- &= \frac{(e^{kw} - 1)ke^{qw}}{(q - k)(1 - e^{(k+q)w}) + (k + q)(e^{kw} - e^{qw})}. \end{aligned}$$

We now need to find the potential/pressure from the equation

$$\nabla\phi = \left( -\rho en + \frac{\eta}{en}\Delta \right) \mathbf{v}, \quad (27)$$

which only the terms  $\exp(\pm ky)$  contribute:

$$\phi(x, y) = \frac{I\rho}{2\pi} \int_{-\infty}^{\infty} e^{ikx} \left[ a_+(k)e^{ky} - a_-(k)e^{-ky} \right] \frac{dk}{k}. \quad (28)$$

In particular, it gives in the Ohmic limit

$$\phi(x, y) = \frac{I\rho}{2\pi} \int_{-\infty}^{\infty} e^{ikx} \left[ (1 + e^{kw})^{-1} e^{ky} - (1 + e^{-kw})^{-1} e^{-ky} \right] \frac{dk}{k}. \quad (29)$$

The voltage  $V = \phi(w, x) - \phi(0, x)$  due to (28) is as follows:

$$V(x) = \frac{I\rho}{\pi} \int \frac{dk}{k} \frac{e^{ikL}(e^{qw} - 1)(e^{kw} - 1)q}{(k + q)(e^{qw} - e^{kw}) + (q - k)(e^{(k+q)w} - 1)}. \quad (30)$$

The dimensionless control parameter, which governs the respective roles of resistivity versus viscosity is  $\epsilon = \rho(n\epsilon\nu)^2/\eta$ . For microfluidic flows between two plates separated by the distance  $h$  the respective parameter is  $\epsilon = 12w^2/h^2$ . Remind that for  $\epsilon = 0$  the resistance  $R(x) = V(x)/I$  is given by (20), which is everywhere negative. In the Ohmic limit,  $\epsilon \rightarrow \infty$ , we have  $qw \rightarrow \infty$  and the resistance is everywhere positive:

$$\lim_{\epsilon \rightarrow \infty} R = \frac{\rho}{\pi} \int \frac{e^{2ikx} dk}{k} \tanh(kw) = \frac{\rho}{\pi} \ln[\coth(\pi L/2w)]. \quad (31)$$

With both  $\eta$  and  $\rho$  nonzero, the resistance changes sign at  $x \simeq \sqrt{\eta/\rho(en)^2}$ . At larger distances, resistance is positive since resistivity dominates. Indeed, the asymptotic at  $x \gg \sqrt{\eta/\rho(en)^2}$  is determined by the same integral (31):

$$\lim_{\rho x^2/\nu \rightarrow \infty} R = \frac{\rho}{\pi} \left( 1 - e^{-w\epsilon n \sqrt{\rho/\eta}} \right) \ln[\coth(\pi L/2w)] > 0 \quad (32)$$

The exponential in both (31,32) at  $x \gg w$  is the same as in the purely Ohmic case. Viscosity dominates at smaller distances: (30) is close to (20) for  $L \ll \sqrt{\eta/\rho(en)^2}$  so that the resistance is negative. Viscosity is a singular perturbation (as a coefficient in front of the highest derivative). That means quite dramatic dependence  $R(x)$  for small  $\eta$ : as one approaches the electrode, the resistance grows to higher and higher positive values as  $R(x) \propto \ln(1/x)$  and then drops fast and goes negative as  $R(L) \propto -x^{-2}$  for  $x \ll \sqrt{\eta/\rho(en)^2}$ .

Remind that the solution (30) is obtained for a point electrode and no-slip boundary conditions. One possible regularization of the non-integrable singularity  $x^{-2}$  is to make the entering current distributed over a finite arc. The case of a Lorentzian distribution is considered in the main text. Another option is to make the electrodes finite:  $v_y(x, 0) = v_y(x, w) = 3I(\ell^2 - x^2)/4\ell^3$ . That makes the nonlocal resistance positive at small distances:

$$R(x) \approx \frac{3\eta}{2\pi(n\epsilon x)^2} \ln \left( \frac{w}{|x^2 - \ell^2|} \right). \quad (33)$$

It is finite for any  $x$  except the ends of the electrodes where it has an integrable singularity. For a finite electrode, negative resistance appears only for sufficiently

large viscosity,  $\eta > \rho(ne\ell)^2/$ . Another generalization of the boundary conditions is to allow a slip at the boundary with the velocity proportional to the electric field:  $v_x = -\partial_y\psi(y=0) = \alpha(x)\partial_x\phi(y=0)$ . Here the surface slip factor  $\alpha$  can be space-dependent (which can model modulation of the surface shape or of its chemical composition). For a constant  $\alpha$ , the potential is renormalized as follows:

$$\phi_k(0) = \frac{I\eta}{\pi(ne)^2} \frac{k \tanh(kw/2) \sinh kw}{kw + \sinh kw + 2(\eta\alpha/ne)k^2 \sinh kw} . \quad (34)$$

It gives a finite value of  $\phi(0,0)$  and is positive at  $L < \sqrt{\eta\alpha/ne}$ . Adding a small periodic component to  $\alpha$ , one obtains a modulation of  $\phi(x,0)$  with the same period i.e. a chain of vortices.

We close with a general remark: bi-harmonic equation in the viscous case is not conformal invariant in distinction from the harmonic equation in the Ohmic case. In particular, this absence of conformal invariance is manifested in the nonlocality of the response. Nonlocal resistance, which exponentially decays in the Ohmic case, in the viscous case is sensitive to neutral modes.